Bone 153 (2021) 116178

Contents lists available at ScienceDirect

Bone

journal homepage: www.elsevier.com/locate/bone

Full Length Article

Deletion of the sodium/hydrogen exchanger 6 causes low bone volume in adult mice

Daniela Schnyder [a,b,c,1], Giuseppe Albano [a,b,c,1], Patrycja Kucharczyk [a,b,c], Silvia Dolder [b,c], Mark Siegrist [b,c], Manuel Anderegg [a,b,c], Ganesh Pathare [a,b,c], Willy Hofstetter [b,c], Roland Baron [d,e], Daniel G. Fuster [a,b,c,*]

[a] Department of Nephrology and Hypertension, Inselspital, Bern University Hospital, University of Bern, Bern, Switzerland
[b] National Centre of Competence in Research (NCCR) TransCure, University of Bern, Bern, Switzerland
[c] Department for BioMedical Research (DBMR), University of Bern, Bern, Switzerland
[d] Division of Bone and Mineral Research, Harvard Medical School and Harvard School of Dental Medicine, Boston, MA, USA
[e] Department of Oral Medicine, Infection and Immunity, Harvard Medical School and Harvard School of Dental Medicine, Boston, MA, USA

ARTICLE INFO

Keywords:
Osteoblasts
Osteoclasts
Osteocytes
Sclerostin
Bone histomorphometry
Bone μCT
Bone formation

ABSTRACT

The sodium/hydrogen exchanger 6 (NHE6) localizes to recycling endosomes, where it mediates endosomal alkalinization through K^+/H^+ exchange. Mutations in the *SLC9A6* gene encoding NHE6 cause severe X-linked mental retardation, epilepsy, autism and corticobasal degeneration in humans. Patients with *SLC9A6* mutations exhibit skeletal malformations, and a previous study suggested a key role of NHE6 in osteoblast-mediated mineralization. The goal of this study was to explore the role of NHE6 in bone homeostasis. To this end, we studied the bone phenotype of NHE6 knock-out mice by microcomputed tomography, quantitative histomorphometry and complementary *ex vivo* and *in vitro* studies.

We detected NHE6 transcript and protein in both differentiated osteoclasts and mineralizing osteoblasts. *In vitro* studies with osteoclasts and osteoblasts derived from NHE6 knock-out mice demonstrated normal osteoclast differentiation and osteoblast proliferation without an impairment in mineralization capacity. Microcomputed tomography and bone histomorphometry studies showed a significantly reduced bone volume and trabecular number as well as an increased trabecular space at lumbar vertebrae of 6 months old NHE6 knock-out mice. The bone degradation marker c-terminal telopeptides of type I collagen was unaltered in NHE6 knock-out mice. However, we observed a reduction of the bone formation marker procollagen type 1 N-terminal propeptide, and increased circulating sclerostin levels in NHE6 knock-out mice. Subsequent studies revealed a significant upregulation of sclerostin transcript expression in both primary calvarial cultures and femora derived from NHE6 knock-out mice.

Thus, loss of NHE6 in mice causes an increase of sclerostin expression associated with reduced bone formation and low bone volume.

1. Introduction

The endoskeleton of land vertebrates is mainly composed of hydroxyapatite (Ca5(PO4)3OH) [1]. Both synthesis and degradation of hydroxyapatite by osteoblasts and osteoclasts, respectively, are highly regulated, pH-dependent processes. Hydroxyapatite formation causes a massive release of H+ ions, in contrast, its dissolution requires acidification. Hence, not surprisingly, both mineralizing osteoblasts and bone degrading osteoclasts are equipped with powerful H+ and HCO3− transport systems, including the V-ATPase, Cl−/HCO3− exchangers and Na+/H+ exchangers (NHEs) [2]. Mineralizing osteoblasts exhibit high NHE activity [3]. While NHE1 expression was observed along the entire plasma membrane, NHE6 seemed to be enriched at the basolateral surface of calcifying osteoblasts, indicating that NHE6 may play a role in the transcellular disposal of H+ ions which are released during hydroxyapatite formation [3]. Two additional NHE isoforms, NHE3 and

* Corresponding author at: Department of Nephrology and Hypertension, Inselspital, Bern University Hospital, Freiburgstrasse 15, 3010 Bern, Switzerland.
E-mail address: Daniel.Fuster@dbmr.unibe.ch (D.G. Fuster).
[1] Contributed equally.

https://doi.org/10.1016/j.bone.2021.116178
Received 6 April 2021; Received in revised form 4 September 2021; Accepted 5 September 2021
Available online 8 September 2021

NHE4, have been detected in human bone-derived osteoblasts [4,5]. The functional role of individual NHEs in osteoblasts, however, remains unknown at the moment.

In bone degrading osteoclasts, transcellular H+ transport occurs in the opposite direction compared to osteoblasts [6]. H+ ions are secreted into the resorption lacuna at the bone surface by the V-ATPase at the apical membrane and HCO3− exits at the basolateral membrane by the Cl−/HCO3− exchanger isoform AE2 [7]. Both resorbing and non-resorbing osteoclasts also exhibit significant NHE activity, and non-selective NHE inhibition by amiloride or its derivatives seems to attenuate osteoclast differentiation and reduce adhesion of osteoclasts to mineralized surfaces [8–11]. Osteoclasts were previously shown to express the two NHE isoforms NHE1 and NHA2 at the basolateral membrane [12,13]. To our knowledge, rigorous in vitro and in vivo studies with transgenic mice were only performed for the NHA2 isoform thus far [13]. Thus, as in osteoblasts, the expression pattern of currently known NHE isoforms as well as the contribution of individual NHEs to osteoclast function remains unknown at the moment.

NHE6 is primarily present in recycling endosomes, where it mediates endosomal alkalinization through K^+/H^+ exchange and is essential for clathrin-mediated endocytosis, receptor recycling and endosomal signaling [14–16]. In a few specialized cells, it has a major plasmalemmal distribution, *e.g.* in cells of the inner ear where it is critical for normal hearing [17,18], or as outlined above, in osteoblasts [3]. Receptor for activated C kinase 1 (RACK1)-dependent translocation of NHE6 from endosomes to the plasma membrane was recently shown to induce endosomal acidification, suggesting physiological regulation of endosomal pH by variation of endosomal NHE6 abundance [19,20].

Nonsense and missense variants as well as deletions in the *SLC9A6* gene encoding the NHE6 isoform cause severe X-linked mental retardation, epilepsy, autism and corticobasal degeneration with tau deposition in affected males [21–24]. Female carriers of pathogenic *SLC9A6* variants also exhibit neurocognitive deficits. To date, only little information is available about the consequences of pathogenic *SLC9A6* gene variants in humans or of NHE6 gene disruption in mice outside the central nervous system. Christianson et al. reported skeletal malformations including long and narrow face, straight nose, square prognathic jaw, large ears and narrow chest in affected family members suggesting a possible role of NHE6 in bone turnover [21].

Given the importance of endocytosis in both osteoclasts and osteoblasts, the previously suspected involvement of NHE6 in osteoblast-mediated bone formation and reports on skeletal malformations in patients with pathogenic SLC9A6 gene variants, we hypothesized that NHE6 may play a critical role in osteoblast and/or osteoclast physiology. The goal of this study was to i) explore the expression pattern of NHE isoforms in osteoblasts and osteoclasts and to ii) examine the role of NHE6 in bone homeostasis.

2. Material and methods

Unless specified otherwise, all chemicals and reagents were obtained from Sigma.

2.1. Animal studies

All animal experiments were in accordance with the Swiss Animal Welfare Law, approved by the Local Veterinary Authority Bern (Veterinäramt Bern; permits # 21/13 and 23/16) and complied with the ARRIVE guidelines. Mice had free access to water and standard chow diet (#3436 from Provimi Kliba AG, Kaiseraugst, Switzerland) and were maintained on a 12 h light/12 h dark cycle. Mice with a targeted Nhe6 gene disruption (Jackson Laboratories Stock# 005843, strain name B6.129P2-Slc9a65tm1Dgen) were obtained from Steven Walkley, Albert Einstein College of Medicine, Bronx, NY, USA. All mice were back-crossed for >10 generations into a C57Bl6/J background.

2.2. Micro-CT analysis

Bone structure was determined in a μCT40 System (Scanco, Brüttisellen, Switzerland) as described [20]. Freshly excised bone specimens were fixed in 4% paraformaldehyde, rinsed overnight with tap water and immersed in 70% ethanol. MicroCT scans were performed in 70% ethanol at the highest resolution, with a voxel size of 6 μm [25].

2.3. Osteoclasts

Primary osteoclasts were prepared from M-CSF dependent non-adherent osteoclast progenitor cells (OPCs) as described [19,23]. Briefly, femora and tibiae of 14-week-old mice were dissected and bone marrow cells flushed out with Hanks Balanced Salt Solution (HBSS) supplemented with 100 U/ml penicillin and 100 U/ml streptomycin. Cells were cultured overnight in α-MEM containing 10% heat inactivated FBS and 30 ng/ml M-CSF. Non adherent cells were then sedimented, resuspended, counted and plated at a density of 4×10^5 cells per ml in α-MEM supplemented with 10% FBS in the presence of 30 ng/ml M-CSF (Chiron, Emeryville, CA) and 20 ng/ml RANKL with medium changes every 3 days. Resorptive capacity of osteoclasts was assesses as described [7,20]. Solutions of 0.12 M Na_2HPO_4 and 0.2 M $CaCl_2$ in 50 mM Tris/HCl pH 7.4 were preincubated overnight in a 5% CO_2 incubator at 37 °C. Equal volumes were mixed and a CaP slurry precipitated. After washing twice with water, the slurry was resuspended in 1 ml of water/90 μl slurry. To the CaP suspension, $^{45}CaCl_2$ (PerkinElmer, Schwerzenbach, CH) was added to a specific activity of 1700 Bq/20 μg slurry. Of the spiked suspension, 200 μl was distributed into wells of 48-well plates, dried at room temperature for 3 days, and baked at 80 °C for 3 h. Before use, the CaP-coated plates were equilibrated with 30% FBS in cell culture medium overnight. Osteoclasts were generated in cultures of OPC for 4 days with M-CSF (30 ng/ml) and RANKL (20 ng/ml) in 5-cm-diameter petri dishes (Avantor, Radnor PA, USA). Mature osteoclasts were detached from the dishes by adding PBS with 0.02% EDTA and incubating the plates at 37 °C. The cells from one petri dish were resuspended in 417 μl αMEM/FBS and 50 μl was distributed into the CaP-coated 48-well plates containing 200 μl αMEM/FBS/M-CSF/RANKL with 15 mM HCl. After 24 h, the cell supernatants were collected and the solubilized ^{45}Ca was counted in a scintillation counter.

2.4. Osteoblasts

Isolation of primary osteoblasts from calvaria of was performed as described [7]. Primary murine osteoblasts were isolated by sequential collagenase digestion of calvariae from 1 to 2-day-old mice and digested for 5 × 20 min with 3 mg/ml collagenase type II (Worthington, NJ, USA) in HBSS. Fractions containing osteoblasts were pooled and 106 cells were seeded into 75-cm^2 culture flasks and in α-MEM supplemented with 10% FBS. After 4 days, cells were aliquoted to 10^6 cells per ml and frozen. Before experiments, cells were expanded in culture medium for 4 days and subsequently plated to 4×10^4 cells per ml. Induction with osteogenic induction medium, staining for alkaline phosphatase activity and quantification of mineralization nodules with Alizarin red S staining were performed as described in detail previously [16,26].

2.5. Osteoblast – osteoclast co-cultures

Osteoclast formation in mouse co-cultures were essentially performed as described [7,15]. On day 0, 4×10^3 osteoblasts and 4×10^4 OPCs, isolated as described above, were seeded in 96 well plates, containing α-MEM supplemented with 10% FBS, 10 nM 1,25-$(OH)_2$ vitamin D3 and recombinant murine TNFα (0.5 ng/ml; Genentech, San Francisco, USA). Medium was then changed every third day and osteoclast differentiation assessed at days 3 to 6 by measuring TRAP activity and counting of TRAP+ multinucleated cells (MNC; ≥3 nuclei/cell).

2.6. Bone histomorphometry

Fixed bones stored in 70% ethanol were dehydrated with graded acetone and embedded in methyl methacrylate. Undecalcified frontal plane lumbar vertebra sections were cut at 4 μm thickness by microtome (RM2255, Leica, Germany). The first section was stained with Von Kossa to identify mineralized bone. The second section was stained with 2% Toluidine Blue (pH 3.7) for the analysis of osteoblasts (Ob.S/BS, N.Ob/BS), and osteoid tissue (OS/BS, O.Th.). The third section was used to stain with Tartrate-Resistant Acid Phosphatase (TRAP) for analysis of osteoclast numbers and surface (Oc.S/BS, N.Oc/BS). The sections were viewed with the Nikon E800 microscope equipped with an Olympus DP71 digital camera. Von Kossa image capture was performed using Olympus CellSens software under 2× magnification or otherwise specified by scale bar. The bone histomorphometric data was obtained at 20× magnification, in a normalized region of interest (ROI) located 200 μm away from the growth plate. The OsteoMeasure analyzing software (Osteometrics Inc., Decatur, GA, USA) was used to generate and calculate the data. The parameters are presented according to the standardized nomenclature [43].

2.7. RNA isolation, RT-PCR and quantitative real-time PCR

RNA extraction from femora was performed as described [27]. RNA extraction of cultured cells, reverse transcription and realtime PCR using pre-synthesized Taqman®-based Assays-on-Demand (Life Technologies/ABI, Rotkreuz, CH) were performed as described previously [20]. The following Assays-on-Demand were employed: Alkaline phosphatase (Mm00475831_m1), Osteocalcin (Mm03413826_mH), Osteoprotegerin (Mm00435454_m1), NHE6 (Mm00555445_m1), Calcitonin receptor (Mm00432282_m1), Cathepsin K (Mm00484039_m1), Sclerostin (Mm00470479_m1), Osterix (Mm04933803_m1), Runx2 (Mm00501584_m1), CCAAT/enhancer binding protein α (Mm00514283_s1), GAPDH (Mm99999915_g1). CT values for triplicate technical replicates were averaged and the amount of mRNA relative to GAPDH calculated using the ΔCt method.

2.8. Antibodies and immunoblotting

Antibodies used in the study were from the following sources: monoclonal anti-transferrin receptor (Invitrogen, Waltham, MA, USA), monoclonal anti-early endosomal antigen 1 (BD Biosciences, Franklin Lakes, N.J., USA), monoclonal anti-GAPDH Mouse (Sigma-Aldrich, St. Louis, MO, USA). Generation and characterization of the rabbit ani-NHE6 antibody has been described [44]. Immunoblotting and quantification were performed as described [45].

2.9. Subcellular fractionation

Subcellular fractionation was essentially performed as described [13,28]. At day 4 of differentiation, osteoclasts derived from WT mice were lysed and the homogenate subjected to fractionation. Fractions were collected from top (#1) to bottom (#15) after centrifugation of cell homogenates (1 mg protein/gradient) on a linear sucrose gradient for 18 h at 200,000 ×*g*. Fractions were then analyzed by immunoblotting.

2.10. Bone turnover markers, plasma electrolytes and renal function parameters

Procollagen type 1 N-terminal propeptide (P1NP) in serum was quantified by P1NP EIA (Immunodiagnostic systems, Boldon, United Kingdom), C-terminal telopeptides of type I collagen (CTX) in serum was quantified by RatLaps™ (CTX-I) EIA (Immunodiagnostic systems), parathyroid hormone (PTH) in plasma was quantified by the Mouse Intact PTH 1–84 Elisa kit (Quidel, San Diego, CA, USA), sclerostin in serum was quantified by Mouse/Rat SOST/Sclerostin Quantikine ELISA Kit (# MSST00; R&D Systems, Minneapolis, MN, USA), c-terminal and intact FGF-23 in plasma were measured by Mouse/Rat FGF-23 C-term ELISA kit (#60-6300) and Mouse/Rat FGF-23 Intact ELISA kit (#60-6800), respectively (Immutopics, San Clemente, CA, USA). Measurements of plasma electrolytes, creatinine and urea were done at the Central laboratory of the Bern University Hospital [46].

2.11. NHE transport activity

NHE activity was measured fluorometrically using the intracellularly trapped pH-sensitive dye BCECF with the NH_4Cl prepulse technique as described previously [29]. Cells grown on glass coverslips were loaded with 1 μM BCECF-AM and exposed to 25 mM NH_4Cl for 15 min in a buffer containing in mM: 120 NaCl, 5 KCl, 2 $CaCl_2$, 1.5 $MgCl_2$, 25 NH_4Cl, 30 Hepes titrated to pH 7.4 with NMDG. Then, cells were washed 3× with and incubated in a buffer containing in mM: 120 Tetramethylammonium-Cl (TMACl), 5 KCl, 2 $CaCl_2$, 1.5 $MgCl_2$, 30 Hepes titrated to pH 7.4 with NMDG. Recording was started and after 60 s cells were rapidly exposed to a buffer containing in mM: 120 NaCl, 5 KCl, 2 $CaCl_2$, 1.5 $MgCl_2$, 30 Hepes titrated to pH 7.4 with NMDG. BCECF fluorescence signals (λ excitation: 490 and 440 nm, λ emission: 535 nm) were recorded in a computer-controlled spectrofluorometer (Fluoromax-2, Photon Technology International). The 490/440 nm fluorescence ratio was calibrated to pHi using the K^+/nigericin method, and initial rate (Vmax; ΔpH/Δtime) of sodium-dependent intracellular pH recovery calculated. [29]. All steps of incubation, recording and calibration were performed at 37 °C. Comparisons were always made between cells studied on the same day.

2.12. Statistical analysis

For comparisons between groups the unpaired Student's *t*-test (two groups) or one-way ANOVA with Tukey post-hoc test (multiple groups) was used. Data were analyzed using GraphPad Prism 8.4 (GraphPad Software, San Diego, CA, USA). All statistical tests were two-sided and $p < 0.05$ was considered statistically significant. Unless stated otherwise, data are shown as means and error bars indicate SD.

3. Results

3.1. Spectrum of NHE isoform expression in osteoclasts and osteoblasts

Currently, 13 NHE paralogs (SLC9 gene family) have been identified in mammalian genomes, encompassing nine SLC9A family members NHE1 – NHE9 (or SLC9A1-SLC9A, respectively), two SLC9B subfamily members NHA1 and NHA2 (or SLC9B1 and SLC9B2, respectively), and two SLC9C subfamily members SLC9C1 (or sperm NHE) and SLC9C2 [30]. SLC9C2 is a putative NHE for which no data currently exist. We analyzed the mRNA expression pattern of 12 NHE isoforms (excluding SLC9C2) in mature murine osteoclast derived from macrophage colony-stimulating factor (M-CSF) dependent non-adherent osteoclast progenitor cells (OPCs) as well as in mineralizing murine osteoblasts derived from neonatal calvaria. As shown in Fig. 1A–D, transcripts encoding most of the known NHE isoforms are expressed in both cell types. In osteoclasts, we were unable to detect transcripts of the epithelial NHE isoforms NHE3 and NHE4 and of the sperm NHE. Whereas NHE3 and sperm NHE mRNAs were also undetectable in mineralizing osteoblasts, NHE4 transcript was detectable in osteoblasts. As depicted in Fig. 1A and B, treatment with RANKL led to a significant upregulation of several NHEs, including NHE2, NHE5, NHE7 and the two SLC9B subfamily members NHA1 and NHA2. In contrast, NHE9 was significantly downregulated by RANKL. In mineralizing osteoblasts, we observed upregulation of NHA1 and NHA2, and downregulation of NHE2 and NHE5, compared to osteoblasts not cultured in osteogenic induction medium containing β-glycerophosphate (Fig. 1C, D). In both differentiated osteoclasts and mineralizing osteoblasts, we detected high transcript levels

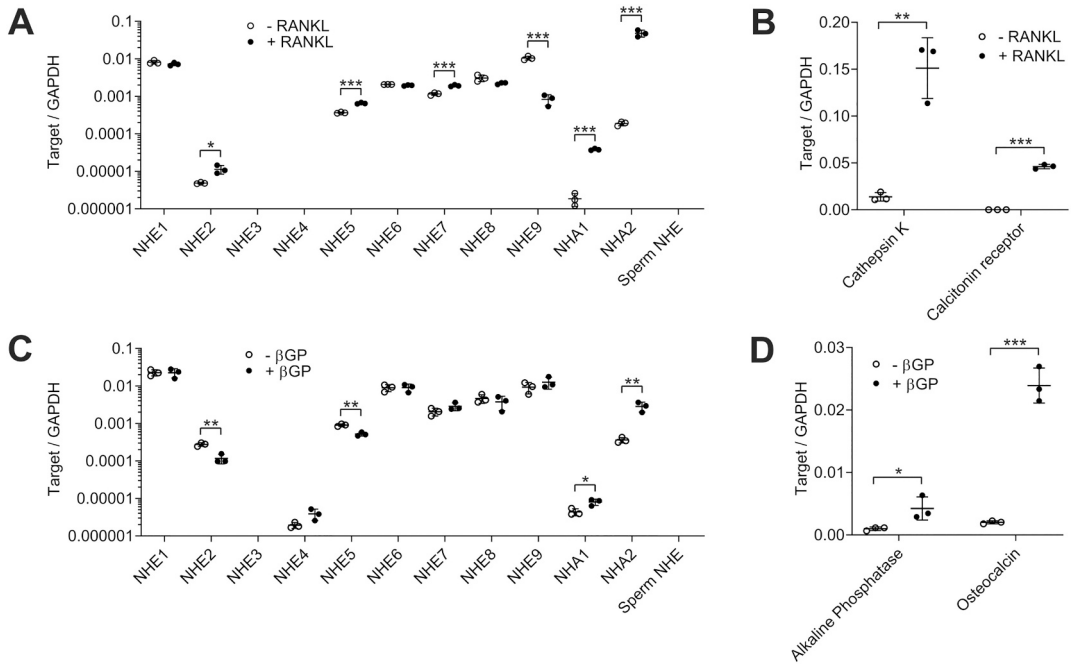

Fig. 1. Expression of NHE isoforms osteoclasts and osteoblasts. A, B) Osteoclasts: Primary M-CSF dependent non-adherent osteoclast progenitor cells (OPCs) were cultured with or without RANKL for 4 days. B) Controls for RANKL dependent osteoclast development. C, D) Osteoblasts: primary osteoblasts isolated from calvaria of 1–2 days old mice were cultured for 28 days with (osteogenic medium) or without 10 mM β–glycerophosphate (β–GP). D) Controls for osteogenic induction. The abundance of target mRNA relative to GAPDH mRNA was calculated using the ΔCt method. Values are shown as means ± SD; $*p < 0.05$, $**p < 0.01$, $***p < 0.001$.

of intracellular NHE isoforms, including NHE6, NHE7, NHE8 and NHE9.

3.2. Role of NHE6 in osteoclasts

As outlined earlier, the main goal of this study was to determine the role of NHE6 in bone homeostasis. We first set out to determine the role of NHE6 in osteoclast differentiation and function. To this end, NHE6 expression was assessed during RANKL-induced osteoclast differentiation in OPCs isolated from wild-type (WT) and NHE6 knock-out (KO). OPCs were cultured in the presence of 20 ng/ml RANKL and 30 ng/ml

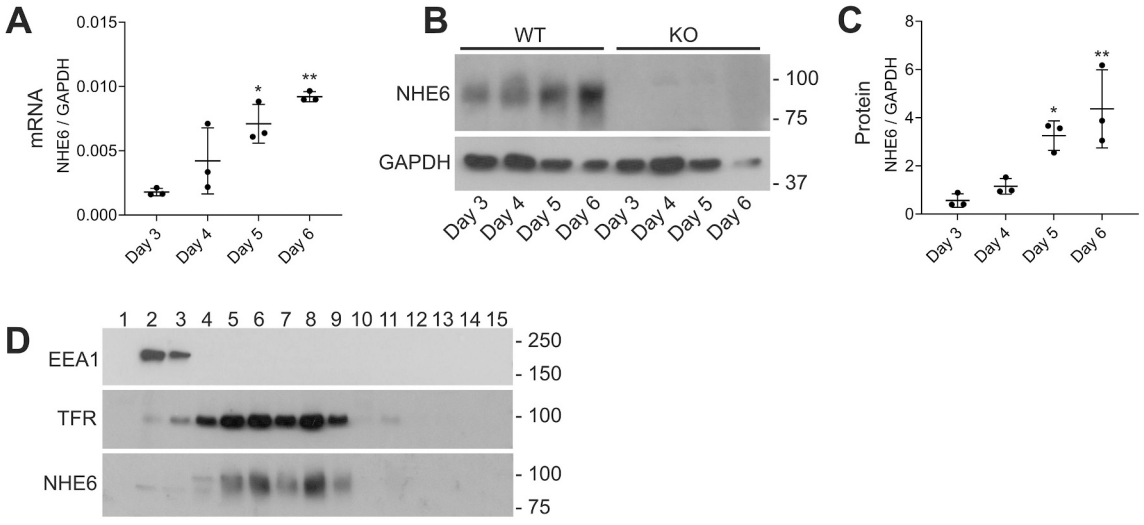

Fig. 2. Expression of NHE6 during osteoclast differentiation. Primary M-CSF dependent non-adherent osteoclast progenitor cells (OPCs) were cultured in the presence of 20 ng/ml RANKL and 30 ng/ml M-CSF for up to 6 days. A) NHE6 transcript expression during osteoclast differentiation. At day 3 to day 6 of differentiation, cells were lysed, mRNA isolated and target gene expression quantified by real-time PCR analysis using Taqman probes. No NHE6 transcript was detectable in osteoclasts from NHE6 KO mice (not shown). The abundance of NHE6 mRNA relative to GAPDH mRNA was calculated using the ΔCt method. Values are shown as means ± SD; $*p < 0.05$ and $**p < 0.01$ compared to day 3.

B, C) NHE6 protein expression during osteoclast differentiation in osteoclasts derived from WT and NHE6 KO mice. At day 3 to day 6 of differentiation, cell lysates were prepared and equal amounts of protein (50 μg) were separated by SDS-PAGE and probed with indicated antibodies. B) Representative immunoblot of WT and NHE6 KO osteoclasts. No NHE6 protein was detected in osteoclasts derived from NHE6 KO mice. C) Quantification of immunoblots of three independent experiments. NHE6 protein expression relative to GAPDH, normalized to day 3 vehicle treatment. Values are shown as means ± SD; $*p < 0.05$ and $**p < 0.01$ compared to day 3.

D) Localization of NHE6 in osteoclasts assessed by subcellular fractionation. EEA1: Early endosomal antigen; TFR: Transferrin receptor. Equal volumes of each fraction were loaded per lane. Experiment shown is representative of 3 individual experiments.

M-CSF for a total of 6 days. As shown in Fig. 2A–C, NHE6 mRNA and protein increased in OPCs with RANKL treatment. No NHE6 mRNA (not shown) or protein (Fig. 2B) were detectable in OPCs derived from NHE6 KO mice. In subcellular fractionation experiments, NHE6 co-migrated with the transferrin receptor, a marker of recycling endosomes, as expected from previous studies in other cell types (Fig. 2D) [14,31]. No relevant overlap of the NHE6 signal was detected with the early endosomal marker EEA1. To assess differentiation of WT and NHE6 KO osteoclasts, OPCs treated with 20 ng/ml RANKL and 30 ng/ml M-CSF were harvested at days 3, 4, 5 and 6 of culture, and tartrate-resistant acid phosphatase (TRAP) activity of cell lysates as well as the number of TRAP positive ($TRAP^+$), multinucleated cells (MNC; ≥3 nuclei/cell) were quantified. As shown in Fig. 3A–B, differentiation into mature osteoclasts was unaffected by loss of NHE6. Similarly, induction of osteoclast differentiation markers was not different between the two groups of OPCs (Fig. 3D, E). We then examined the resorptive activity of mature osteoclasts *in vitro*, as described [26,32,33]. Osteoclasts were collected at day 4 of differentiation and seeded into calcium-phosphate (CaP) coated wells, containing ^{45}Ca as a tracer. Resorptive activity was calculated as ^{45}Ca released into the cell culture supernatant, normalized to TRAP activity 24 h after seeding. As shown in Fig. 3C, there was a small but significant decrease of the resorptive activity of NHE6-deficient osteoclasts compared to osteoclasts derived from WT littermate mice.

3.3. Role of NHE6 in osteoblasts

In a next series of experiments, we used primary osteoblasts to study NHE6 expression, proliferation and cell-mediated mineralization *in vitro*. To this end, osteoblasts were cultured in osteogenic induction medium containing β-glycerophosphate [34]. As shown in Fig. 4A–C, NHE6 mRNA and protein were found to be expressed in osteoblast cultures throughout day 28. No NHE6 mRNA (not shown) or NHE6 protein (Fig. 4B, C) were detectable in osteoblasts derived from NHE6 KO mice. During culture, there was a time-dependent increase of NHE6 mRNA expression (Fig. 4A). On protein level, we detected an increase from day 7 to day 14 of culture, but in later culture stages, NHE6 protein expression levels returned to early culture levels (Fig. 4B, C).

Throughout culture day 28, no differences in the expression of osteoblast differentiation markers (Fig. 5A, B), alkaline phosphatase activity (Fig. 5C, D) or viability (Fig. 5E) were apparent between WT and NHE6 KO osteoblasts. To assess the mineralization capacity, osteoblasts were cultured in osteogenic induction medium supplemented with 10 mM β-glycerophosphate for 28 days. Medium without β-glycerophosphate served as negative control. Quantification of mineralization by Alizarin red was performed at days 7, 14, 21 and 28 (Fig. 5C, F). We observed significantly higher mineralization at days 21 and 28 days of culture in osteoblasts derived from NHE6 KO mice compared to osteoblasts derived from WT littermate mice.

We next also conducted osteoblast-osteoclast co-cultures to study the role of NHE6 in osteoblast-osteoclast interactions. To this end, osteoblasts isolated from WT or NHE6 KO mice were co-cultured with OPCs either isolated from WT or NHE6 KO mice. Cells were harvested at days 3, 4, 5 and 6 of culture, and TRAP activity of cell lysates and the number of $TRAP^+$, multinucleated cells were quantified. As shown in Fig. 6A, B, differentiation into mature osteoclasts in the co-culture system was not affected by deficiency of NHE6 in either osteoblasts, OPCs or both cell types.

3.4. NHE transport activity in NHE6 KO osteoblasts

Although NHE6 is an intracellular NHE involved in endosomal pH homeostasis [31], NHE6 was proposed to localize to the plasma membrane in osteoblasts and participate in cytosolic pH homeostasis [3]. We thus assessed plasmalemmal NHE transport activity in WT and NHE6 osteoblasts. To this end, osteoblasts were maximally acidified using the NH_4Cl pre-pulse technique and the sodium-dependent intracellular pH recovery quantified in the presence or absence of the NHE inhibitor amiloride (Fig. 7A, B) [29]. In both WT and NHE6 KO osteoblasts, amiloride completely abrogated NHE activity, suggesting that plasmalemmal NHE transport in WT and NHE6 KO osteoblasts is mediated by the amiloride-sensitive NHE isoform NHE1 [35], which is highly

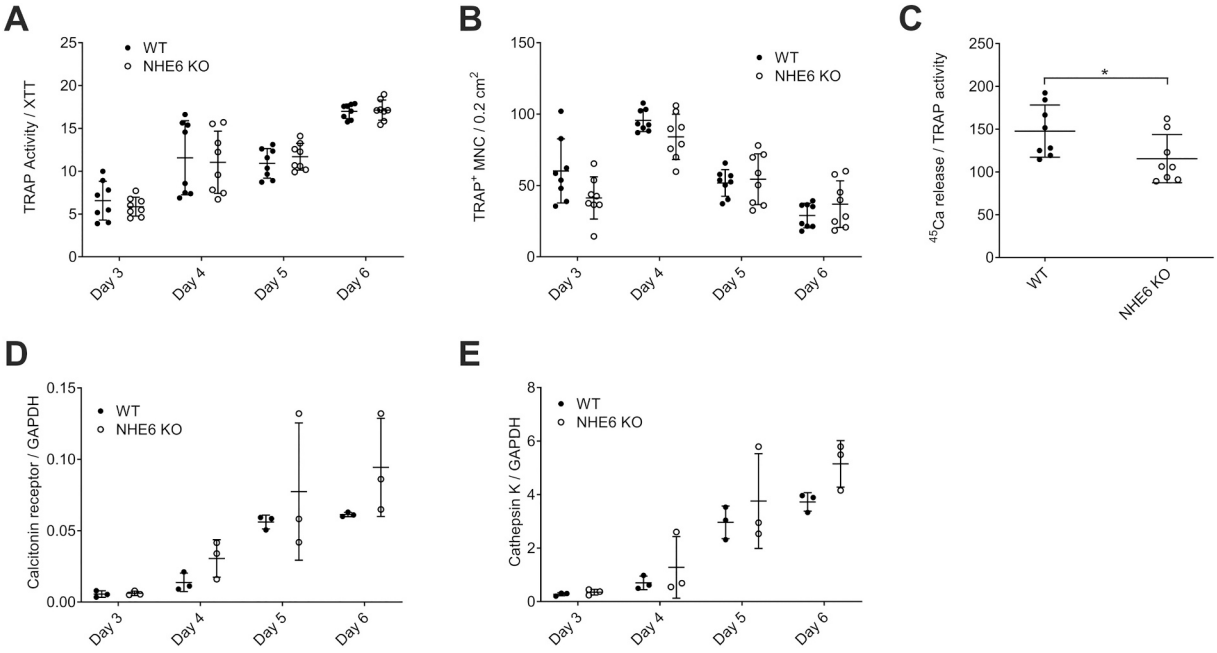

Fig. 3. In vitro characterization of osteoclast differentiation and function. Primary M-CSF dependent non-adherent OPCs isolated from WT and NHE6 KO mice were cultured in the presence of 20 ng/ml RANKL and 30 ng/ml M-CSF for up to 6 days. A) TRAP activity normalized to XTT in OPC cultures harvested at indicated days. B) Quantification of $TRAP^+$ multinucleated cells (MNC; ≥3 nuclei/cell) at indicated days. C) Resorptive activity of osteoclasts at day 4 of RANKL stimulation, quantified as ^{45}Ca released in the supernatant normalized to TRAP activity. D, E) Transcript expression of osteoclast differentiation markers relative to GAPDH, calculated using the ΔCt method. Values are shown as means ± SD; $*p < 0.05$.

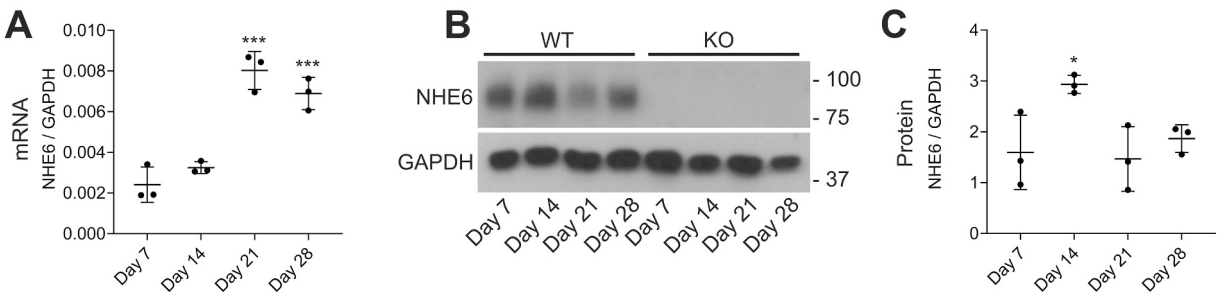

Fig. 4. Expression of NHE6 in osteoblasts. Primary osteoblasts isolated from calvaria of newborn WT or NHE6 KO mice were cultured up to 28 days in osteogenic induction medium containing 10 mM β-GP. A) NHE6 transcript expression. At days 7, 14, 21 and 28 of culture, osteoblasts were lysed, mRNA isolated and target gene expression quantified by real-time PCR analysis using Taqman probes. No NHE6 transcript was detectable in osteoblasts from NHE6 KO mice. The abundance of target mRNA relative to GAPDH mRNA was calculated using the ΔCt method. B, C) NHE6 protein expression during osteoblast proliferation in osteoblasts derived from WT and NHE6 KO mice. At days 7, 14, 21 and 28 of culture, cell lysates were prepared and equal amounts of protein (50 μg) were separated by SDS-PAGE and probed with indicated antibodies. No NHE6 protein was detected in osteoclasts derive from NHE6 KO mice. B) Representative immunoblot. C) Quantification of immunoblots. NHE6 protein expression relative to GAPDH. Values are shown as means ± SD; $*p < 0.05$ compared to day 3.

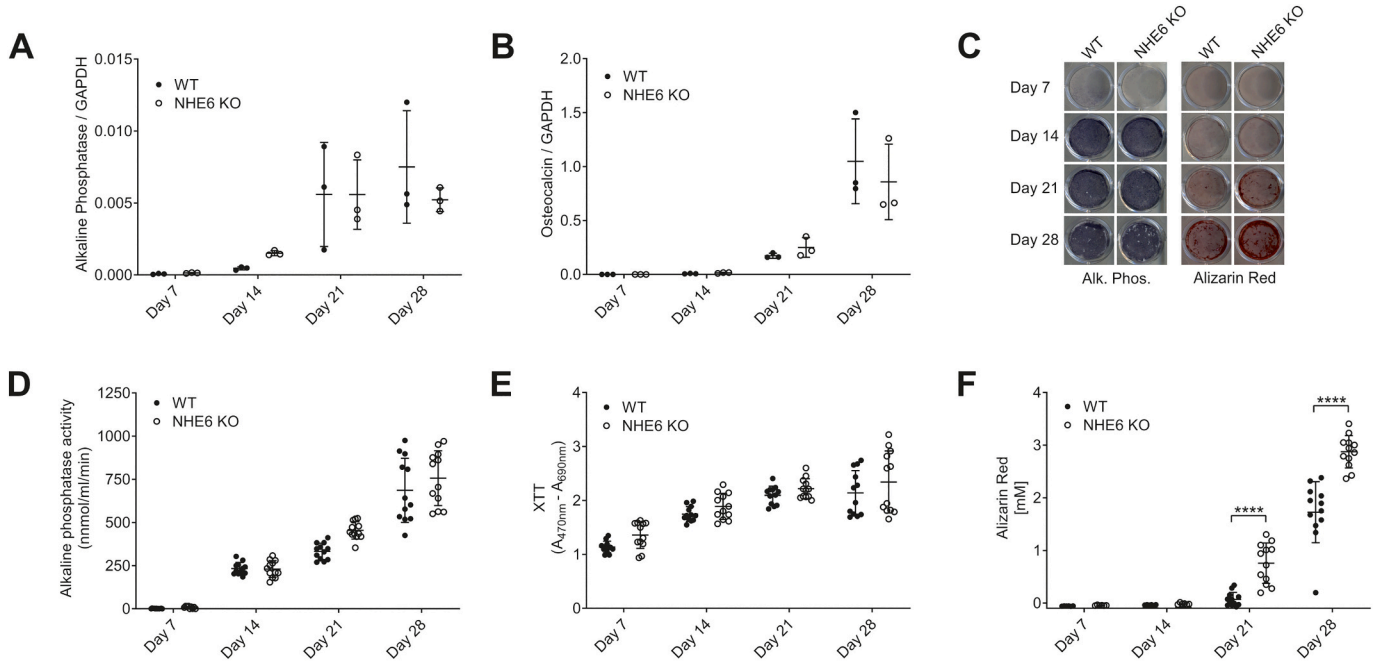

Fig. 5. Expression of osteoblast differentiation markers, alkaline phosphatase activity and mineralization. Primary osteoblasts isolated from calvaria of newborn WT or NHE6 KO mice were cultured up to 28 days in the presence of 10 mM β-GP (osteogenic induction medium). A–B) Alkaline phosphatase and osteocalcin transcript expression. At days 7, 14, 21 and 28 of culture, osteoblasts were lysed, mRNA isolated and target gene expression quantified by real-time PCR analysis using Taqman probes. The abundance of target mRNA relative to GAPDH mRNA was calculated using the ΔCt method. C) Representative images of alkaline phosphatase (left panels) and Alizarin red staining (right panels) in osteoblast cultures at days 7, 14, 21 and 28. D) Quantification of alkaline phosphatase activity in osteoblast cultures at days 7, 14, 21 and 28. E) Assessment of cell viability of osteoblast cultures at days 7, 14, 21 and 28 by XTT assay. F) Quantification of Alizarin red staining in osteoblast cultures by acetic acid extraction and colorimetric detection at 405 nm at days 7, 14, 21 and 28. Values are shown as means ± SD; $****p < 0.0001$.

expressed in both mineralizing and non-mineralizing osteoblasts (Fig. 1B). Furthermore, NHE transport activity was similar between non-mineralizing and mineralizing WT and NHE6 KO osteoblasts, indicating that NHE6 has no role in cytoplasmatic pH regulation in osteoblasts.

3.5. Structural bone parameters assessed by microcomputed tomography in NHE6 KO mice

To determine the impact of the *in vitro* findings observed with osteoblasts and osteoclasts derived from NHE6 KO mice on structural bone parameters, we performed high-resolution microcomputed tomography (micro-CT) studies on lumbar vertebrae of 3 months old male WT and NHE6 KO mice. As depicted in Fig. 8A–D, with the exception of a lower bone volume fraction (BV/TV) at a single site (L4) in NHE6 KO males, we did not detect significant differences in structural bone parameters between the two groups of mice. Based on these findings, we decided to further age cohorts of WT and NHE6 KO mice. As shown in Fig. 8, at 6 months of age, both male (E–H) and female (I–L) NHE6 KO mice displayed a significantly reduced BV/TV and trabecular number as well as an increased trabecular space at all three lumbar vertebral sites studied (L3, L4 and L5). Mean body weight was similar between the two groups of mice at 6 months of age (31.5 g ± 1.8 g WT males and 32.5 g ± 1.4 g NHE6 KO males, $p = 0.588$; 24.1 g ± 1.8 g WT females and 27.3 g ± 2.9 g NHE6 KO females, $p = 0.156$).

3.6. Bone histomorphometry

To further investigate the bone phenotype of NHE6 KO mice, we next

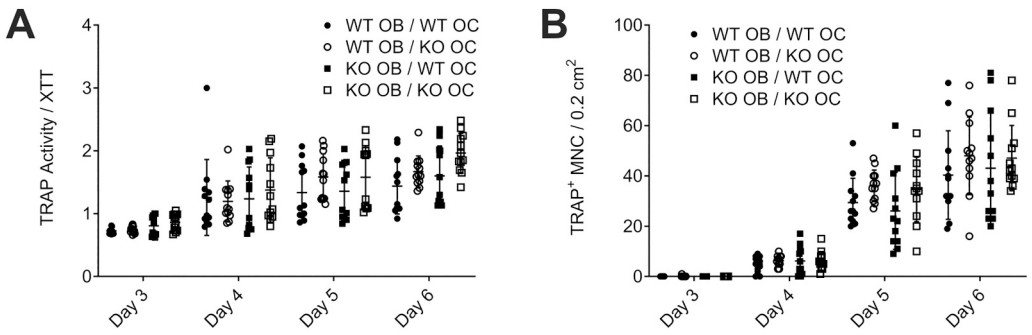

Fig. 6. In vitro osteoclast differentiation in osteoblast-osteoclast co-cultures. Primary OPCs isolated from WT and NHE6 KO mice were co-cultured with osteoblasts isolated from calvaria of newborn WT or NHE6 KO mice for up to 6 days. A) TRAP activity normalized to XTT in OPC cultures harvested at indicated days. B) Quantification of $TRAP^+$ multinucleated cells (MNC; ≥3 nuclei/cell) at indicated days. Values are shown as means ± SD.

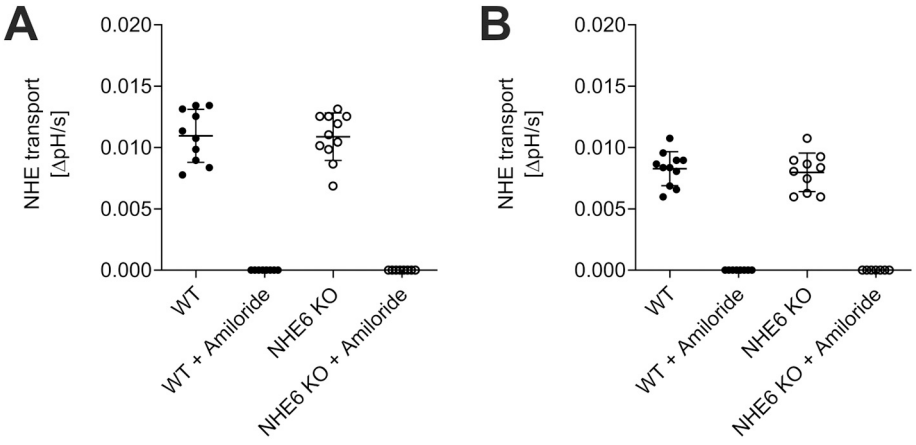

Fig. 7. NHE transport activity in osteoblasts. Measurement of plasma membrane NHE transport activity in non-mineralizing (A) and mineralizing (B) osteoblasts by quantification of the sodium-dependent intracellular pH recovery after acidification of the cytoplasma, in the presence or absence of the NHE inhibitor amiloride (1 mM). Values are shown as means ± SD.

performed bone histomorphometry of lumbar vertebrae in 6 months old WT and NHE6 KO mice (Tables 1, 2). Structural histomorphometry parameters in female NHE6 KO mice confirmed a significant decrease in trabecular bone volume and trabecular numbers with a corresponding increase in trabecular spacing, but no change in trabecular thickness, consistent with osteopenia. These parameters were not significantly modified in NHE6 KO males, albeit a clear trend to decreased BV/TV was observed. When testing the results by two way ANOVA to distinguish the gender effects from the effects of NHE6 KO independently and their interaction (Table 2), NHE6 KO mice exhibited a significant decrease in trabecular bone volume and trabecular numbers with a corresponding increase in trabecular spacing, and no significant change in trabecular thickness compared to WT mice. Despite the expected differences between genders, no significant interaction between gender and genotype was detected, confirming that the effects of NHE6 KO were similar in males and females. In contrast to structural parameters, cellular histomorphometry parameters (osteoclast and osteoblast numbers, osteoid thickness), did not reveal any significant differences between WT and NHE6 KO mice, suggesting that the cellular changes that led to low bone mass occurred at earlier time points, as indicated by the decrease in bone formation marker procollagen type 1 N-terminal propeptide (P1NP) we observed at 3 months of age (Fig. 9A).

3.7. Circulating mineral metabolism markers and gene expression in bone of WT and NHE6 KO mice

We next quantified in 3 months old mice circulating levels of the bone formation marker procollagen type 1 N-terminal propeptide (P1NP) and of the bone degradation marker C-terminal telopeptides of type I collagen (CTX). Serum P1NP levels were significantly lower in NHE6 mice compared to WT mice (Fig. 9A), while CTX levels were similar in both groups of mice (Fig. 9B), suggesting attenuated bone formation as the mechanism for reduced bone volume in NHE6 KO mice. To further investigate the cause of reduced bone formation in NHE6 KO mice, we measured plasma parathyroid hormone (PTH), intact and C-terminal fibroblast growth factor 23 (FGF-23), plasma electrolytes and renal function parameters in WT and NHE6 KO mice. As shown in Fig. 9C–E and Table 3, these studies did not reveal differences between the two groups of mice. However, sclerostin, a bone-derived glycoprotein with anti-anabolic effects on osteoblasts [25,36,37], was significantly elevated in NHE6 KO mice compared to WT mice (Fig. 9F). We next assessed sclerostin transcript expression in primary calvarial cultures derived from WT and NHE6 KO mice *in vitro*. As demonstrated in Fig. 9G, sclerostin transcript expression was significantly upregulated in NHE6 KO cells. To assess sclerostin expression *in vivo*, we isolated RNA of femora from 3 months old WT and NHE6 KO mice, and quantified sclerostin and canonical Wnt pathway target gene transcript expression (Fig. 9H–K). Results obtained indicate elevated sclerostin expression in bone of NHE6 KO mice, in line with elevated circulating sclerostin levels observed in NHE6 KO mice. In addition, we observed upregulation of the osteogenic inducers Runx2 and Osterix in NHE6 KO mice, while no difference was observed between WT and NHE6 KO mice in the expression of the adipogenic inducer CCAAT/enhancer binding protein α [38].

Together, these data suggest that NHE6 KO mice exhibit a cell-autonomous increase of sclerostin expression in bone associated with

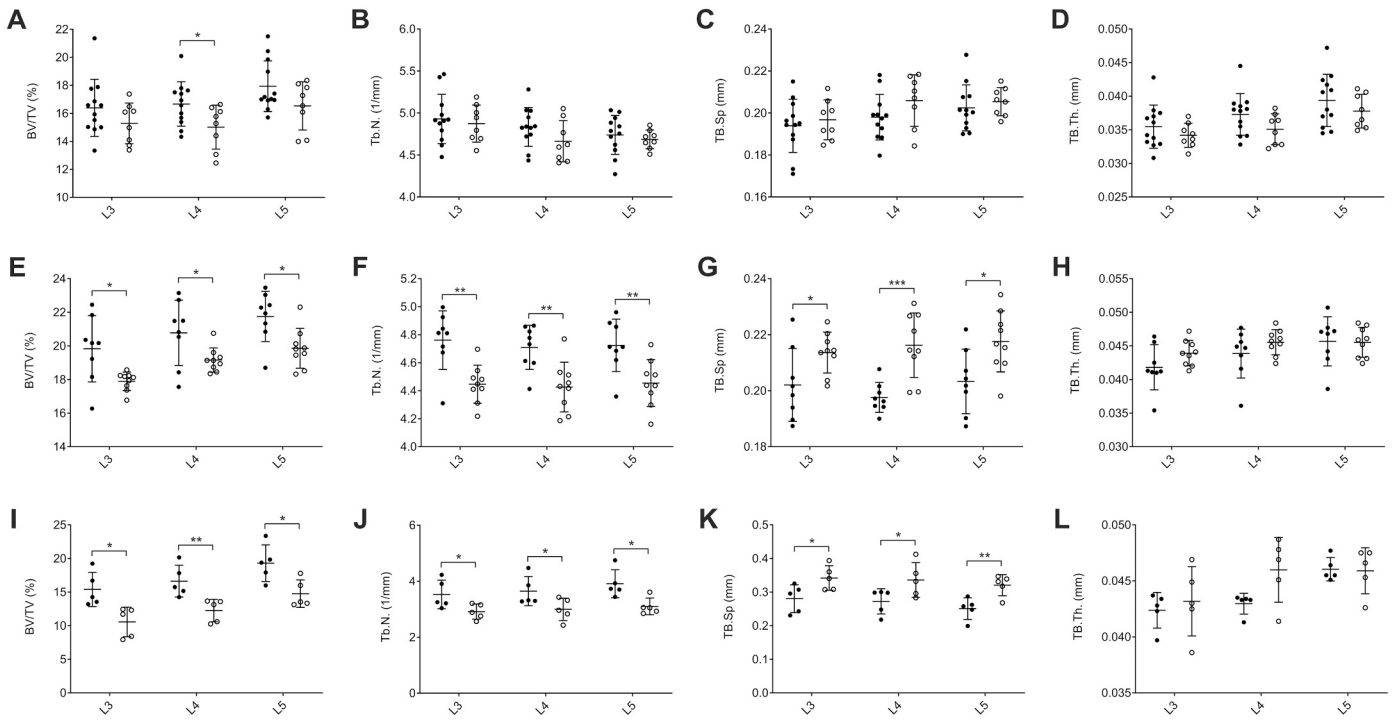

Fig. 8. Structural bone parameters of WT and NHE6 KO mice at 3 and 6 months of age. Lumbar vertebrae (# 3, 4 and 5) at 3 or 6 month of age were isolated and analyzed by μCT. A–D) Histograms representing structural parameters of lumbar vertebrae of 3 months old male mice. E–H) Histograms representing structural parameters of lumbar vertebrae of 6 months old male mice. I–L) Histograms representing structural parameters of lumbar vertebrae of 6 months old female mice. Total volume/bone volume fraction (BV/TV), trabecular number (Tb.N.), trabecular thickness (Tb.Th.), trabecular space (Tb.Sp.). Values are shown as means ± SD; $*p < 0.05$, $**p < 0.01$, $***p < 0.001$.

Table 1
Bone histomorphometry of female and male 6 months old WT and NHE6 KO mice.

Vertebra trabecular parameters	Female, WT ($n = 5$)	Female, KO (n = 5)	Male, WT (n = 5)	Male, KO (n = 5)
BV/TV (%)	16.47 ± 2.45	11.44 ± 3.15*	17.81 ± 3.42	14.60 ± 1.70
Tb.Th (μm)	45.32 ± 2.00	42.14 ± 4.60	42.56 ± 6.51	38.00 ± 2.08
Tb.N (/mm)	3.64 ± 0.51	2.68 ± 0.55*	4.17 ± 0.40	3.84 ± 0.30##
Tb.Sp (μm)	234.84 ± 45.84	346.57 ± 98.71*	199.23 ± 27.43	224.02 ± 22.68#
Ob.S/B.Pm (%)	20.36 ± 5.18	17.98 ± 8.10	10.96 ± 2.00	13.34 ± 3.59
N.Ob/B.Pm (#/mm)	13.52 ± 2.79	12.49 ± 6.39	7.33 ± 1.15	9.59 ± 2.20
OS/BS (%)	9.88 ± 4.21	8.59 ± 6.19	5.24 ± 1.58	7.50 ± 3.10
O.Th (μm)	2.28 ± 0.26	2.61 ± 0.52	2.27 ± 0.45	2.23 ± 0.50
Oc.S/B.Pm (%)	11.17 ± 2.32	11.60 ± 1.44	8.67 ± 1.63	8.91 ± 2.36
N.Oc/B.Pm (#/mm)	5.65 ± 0.76	6.76 ± 1.55	4.33 ± 0.80	4.48 ± 1.00#

Bone volume/total volume fraction (BV/TV), trabecular number (Tb.N.), trabecular thickness (Tb.Th.), trabecular space (Tb.Sp.), osteoblast number/bone perimeter (N.Ob/B.Pm), osteoclast number/bone perimeter (N.Oc/B.Pm), osteoblast surface/bone surface (Ob.S/BS), osteoclast surface/bone surface (Oc.S/BS), osteoid thickness (O.Th), osteoid surface/bone surface (OS/BS).

* $p < 0.05$ statistically significant *vs.* female, WT (Tukey post-hoc test).

\# $p < 0.05$.

\## $p < 0.01$ statistically significant *vs.* female, KO (Tukey post-hoc test).

Table 2
Two-way ANOVA analysis of bone histomorphometry results.

Vertebra trabecular parameters	Female *vs* Male	WT *vs* KO	Interaction between gender and genotype
BV/TV (%)	$P = 0.0872$	$p = 0.0041$	$p = 0.4691$
Tb.Th (μm)	$p = 0.0876$	$p = 0.0583$	$p = 0.7195$
Tb. N (mm)	$P = 0.0007$	$p = 0.0055$	$p = 0.1381$
Tb. Sp (μm)	$P = 0.0071$	$p = 0.0169$	$p = 0.1089$
Ob.S/B.Pm (%)	$p = 0.0085$	$p = 0.9990$	$p = 0.3231$
N.Ob/B.Pm (#/mm)	$p = 0.0144$	$p = 0.7144$	$p = 0.3369$
OS/BS (%)	$p = 0.1401$	$p = 0.7953$	$p = 0.3495$
O.Th (μm)	$p = 0.3433$	$p = 0.4643$	$p = 0.3696$
Oc.S/B.Pm (%)	$p = 0.0097$	$p = 0.7113$	$p = 0.9114$
N.Oc/B.Pm (#/mm)	$p = 0.0018$	$p = 0.2094$	$p = 0.3333$

Bone volume/total volume fraction (BV/TV), trabecular number (Tb.N.), trabecular thickness (Tb.Th.), trabecular space (Tb.Sp.), osteoblast number/bone perimeter (N.Ob/B.Pm), osteoclast number/bone perimeter (N.Oc/B.Pm), osteoblast surface/bone surface (Ob.S/BS), osteoclast surface/bone surface (Oc.S/BS), osteoid thickness (O.Th), osteoid surface/bone surface (OS/BS). Statistical analysis with two-way ANOVA.

an attenuated bone formation rate.

4. Discussion

Our expression analysis reveals that most known NHE isoforms are

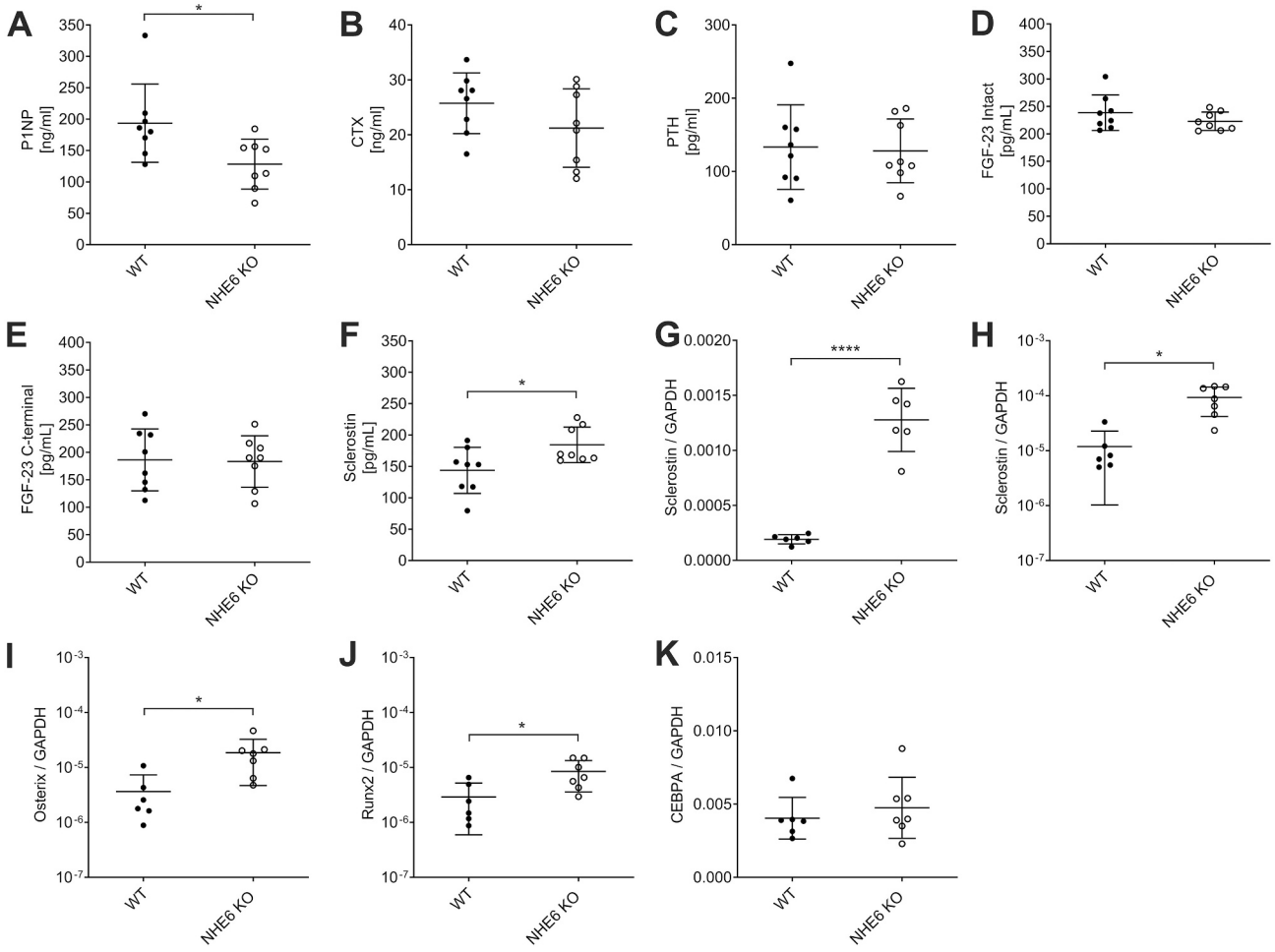

Fig. 9. Circulating mineral metabolism markers and gene expression in bone of WT and NHE6 KO mice at 3 months of age. A) Serum procollagen type 1 N-terminal propeptide (P1NP), B) Serum C-terminal telopeptides of type I collagen (CTX), C) Plasma parathyroid hormone (PTH), D) Plasma Intact fibroblast growth factor 23 (Intact FGF-23), E) plasma C-terminal fibroblast growth factor 23 (C-terminal FGF-23), F) Serum sclerostin, G) Sclerostin transcript expression in primary calvarial cultures, H–K) Sclerostin, Osterix, Runx2 and CCAAT/enhancer binding protein α (CEBPA) transcript expression in femora of 3 months old mice. The abundance of target mRNA relative to GAPDH mRNA was calculated using the ΔCt method. Values are shown as means ± SD; *$p < 0.05$, ****$p < 0.0001$.

Table 3
Blood parameters of WT and NHE6 KO mice.

Plasma parameter (concentration)	WT	NHE6 KO	*p*-Value
Na (mM)	147.25 ± 1.03	147.25 ± 1.83	NS
K (mM)	5.22 ± 0.46	5.8 ± 0.91	NS
Cl (mM)	98.25 ± 1.28	99.5 ± 2.07	NS
Ca (mM)	2.24 ± 0.06	2.26 ± 0.06	NS
P (mM)	2.62 ± 0.32	2.91 ± 0.56	NS
Mg (mM)	0.96 ± 0.07	1.02 ± 0.13	NS
Creatinine (μM)	9.75 ± 1.67	11.5 ± 1.77	NS
Urea (mM)	8.95 ± 1.36	7.72 ± 1.20	NS

Na = sodium, K = potassium, Cl = chloride, Ca = calcium, P = inorganic phosphate, Mg = magnesium. $N = 8$ male mice per genotype, 3 months old. Results shown are mean ± SD. Unpaired *t*-test; NS = not significant.

expressed in the two main cell types of bone, osteoblasts and osteoclasts. Of the plasmalemmal clade (including isoforms NHE1-NHE5), NHE1, NHE2 and NHE5 are the main paralogs expressed. Both NHE2 and NHE5 exhibit differential regulation in the two cell types, being upregulated by RANKL and downregulated in mineralizing osteoblasts. In contrast, all paralogs of the intracellular clade NHE6-NHE9 are abundantly expressed in both cell types. Changes observed were an upregulation of NHE7 and a pronounced ~10× fold downregulation of NHE9 upon RANKL stimulation. Interestingly, both SLC9B subfamily paralogs were not only significantly upregulated in osteoclasts, as reported previously [13,39], but also in mineralizing osteoblasts. Together, these results lay the ground for the exploration of the physiological relevance of individual NHEs in bone biology.

In this study, we focused on the intracellular NHE isoform NHE6. Micro-CT studies of bones isolated from WT and NHE6 KO mice revealed an age-dependent reduction in bone volume of NHE6 KO mice. Alterations in structural bone parameters were confirmed by histomorphometry, and the two-way ANOVA analysis revealed a highly significant effect of NHE6 deletion on bone volume, independent of gender. Although bone volume was lower at 6 months of age, we detected no alterations in cellular histomorphometry parameters in NHE6 KO mice. The reduction of the bone formation marker P1NP in 3 months old NHE6 KO mice indicates that the cellular changes responsible for the significantly reduced bone volume observed in 6 months old NHE6 KO mice occur at an earlier time point. A limitation of this study is the absence of fluorescent labels in bone and dynamic assessment of the rates of mineralization and bone formation. Hence, while our data strongly suggest reduced bone formation as the underlying mechanism, dynamic histomorphometry data will be needed to quantify bone turnover and mineralization.

Experiments performed with primary bone cells derived from WT and NHE6 KO mice revealed subtle differences. The resorptive capacity of NHE6 KO osteoclasts was decreased. In contrast, osteoclast

differentiation assessed by exogenous addition of RANKL to OPCs or in the osteoblast-osteoclast co-culture assay was not affected by loss of NHE6. The basis of the resorptive deficit in NHE6 KO osteoclasts remains unknown at the moment. Vesicular transport along the endo-lysosomal pathway, however, is critical for polarization of osteoclasts and the development of the ruffled border, the resorptive organelle of the osteoclast [40]. Hence it is possible that polarization, development of the ruffled border and/or endosomal signaling are impaired in NHE6-deficient osteoclasts.

Surprisingly, our *in vitro* studies did not reveal an impairment in osteoblast function, as expected [3]. In contrast, our data indicate that proliferation of NHE6-deficient osteoblasts is normal and mineralization increased *in vitro*. The mechanisms responsible for increased mineralization of NHE6-deficient osteoblasts are currently unknown and may be due to alterations in endosomal pH with subsequent changes in endosomal trafficking or signaling. Our studies also indicate that NHE6 is dispensable for cytoplasmic pH regulation in osteoblasts. However, constitutive global KO of NHE6 may result in compensatory changes which mitigate or mask a phenotype. Future studies will need to employ cell-specific and inducible KO models of NHE6 to investigate this further.

The finding of decreased resorptive activity of osteoclasts and increased mineralization of osteoblasts upon loss of NHE6 *in vitro* is difficult to reconcile with the *in vivo* data demonstrating a reduction in the bone formation marker P1NP and an age-dependent lower bone volume in NHE6 KO mice. Our data reveal that there is a cell autonomous increase of sclerostin expression in bone associated with elevated circulating sclerostin levels in NHE6 KO mice. Hence, an increase in sclerostin may be responsible for the bone phenotype observed in NHE6 KO mice. Sclerostin is an osteocyte-derived glycoprotein that functions as antagonist of the canonical Wnt pathway and thereby has anti-anabolic effects on osteoblasts. Surprisingly, our data reveal an increased expression of the osteogenic inducers Runx2 and Osterix in NHE6 KO mice [38]. Upregulation of Runx2 and Osterix may represent a counterregulatory response to elevated sclerostin levels. Alternatively, Runx2 and Osterix may be responsible for the upregulation of sclerostin expression in NHE6 KO mice. Recent data indicate that both Runx2 and Osterix are important inducers of sclerostin expression in bone [41]. The reason for the cell-autonomous increase of sclerostin expression in the bone of NHE6 KO mice remains unclear at the moment, and a limitation of our study is the lack of cellular histomorphometry data on osteocytes. We speculate that endosomal signaling (and hence outside-in signaling) may be altered upon loss of NHE6, resulting in augmented sclerostin mRNA transcription. However, other scenarios are also possible. Thus, both the molecular mechanisms of increased sclerostin expression and the contribution of sclerostin to the bone phenotype observed in NHE6 KO mice remain unclear and further studies are needed to obtain definitive answers.

Our results also have implications for patients with pathogenic *SLC9A6* gene variants or deletions. Low bone mass is associated with increased fracture risk, morbidity and mortality [42]. Certainly, data obtained in rodents cannot be directly extrapolated to humans. However, we believe that our results warrant investigations on bone density, bone turnover markers and sclerostin levels in patients with *SLC9A6*-associated disease. Results of such studies may lay the ground for new diagnostic and preventive measures for patients affected by this rare disease.

CRediT authorship contribution statement

WH, RB and DGF designed the research; DS, GA, SD, MS, MA and GP performed the research; DS, WH, RB and DGF analyzed the data; DS and DGF wrote the paper; all authors approve the final version of the manuscript; DS, WH, RB and DGF accept responsibility for the integrity of data analysis in the manuscript.

Declaration of competing interest

DGF has served as a consultant for Otsuka Pharmaceuticals and Alnylam, and has received unrestricted research funding from Novartis, Abbvie, Otsuka Pharmaceuticals and Boehringer Ingelheim. All other authors have nothing to disclose.

The data that support the findings of this study are openly available in DRYAD (https://doi.org/10.5061/dryad.9w0vt4bdt).

Acknowledgments

This study was supported by the Swiss National Science Foundation (# grants 31003A_152829 and 3100A_172974) and the Swiss National Science Foundation funded National Center for Competence in Research (NCCR Transcure).

References

[1] J.A. Ruben, A.A. Bennett, The evolution of bone, Evolution 41 (1987) 1187–1197.
[2] S.F. Pedersen, L. Counillon, The SLC9A-C mammalian Na(+)/H(+) exchanger family: molecules, mechanisms, and physiology, Physiol. Rev. 99 (2019) 2015–2113.
[3] L. Liu, P.H. Schlesinger, N.M. Slack, P.A. Friedman, H.C. Blair, High capacity Na+/H+ exchange activity in mineralizing osteoblasts, J. Cell. Physiol. 226 (2011) 1702–1712.
[4] A. Mobasheri, S. Golding, S.N. Pagakis, K. Corkey, A.E. Pocock, B. Fermor, M. J. O'Brien, R.J. Wilkins, J.C. Ellory, M.J. Francis, Expression of cation exchanger NHE and anion exchanger AE isoforms in primary human bone-derived osteoblasts, Cell Biol. Int. 22 (1998) 551–562.
[5] M. Numata, K. Petrecca, N. Lake, J. Orlowski, Identification of a mitochondrial Na+/H+ exchanger, J. Biol. Chem. 273 (1998) 6951–6959.
[6] A.V. Rousselle, D. Heymann, Osteoclastic acidification pathways during bone resorption, Bone 30 (2002) 533–540.
[7] J. Wu, L.H. Glimcher, A.O. Aliprantis, HCO3-/Cl- anion exchanger SLC4A2 is required for proper osteoclast differentiation and function, Proc. Natl. Acad. Sci. U. S. A. 105 (2008) 16934–16939.
[8] T.J. Hall, T.J. Chambers, Na+/H+ antiporter is the primary proton transport system used by osteoclasts during bone resorption, J. Cell. Physiol. 142 (1990) 420–424.
[9] T.J. Hall, M. Schaeublin, T.J. Chambers, Na+/H(+)-antiporter activity is essential for the induction, but not the maintenance of osteoclastic bone resorption and cytoplasmic spreading, Biochem. Biophys. Res. Commun. 188 (1992) 1097–1103.
[10] K. Henriksen, M.G. Sorensen, V.K. Jensen, M.H. Dziegiel, O. Nosjean, M.A. Karsdal, Ion transporters involved in acidification of the resorption lacuna in osteoclasts, Calcif. Tissue Int. 83 (2008) 230–242.
[11] H. Kajiya, F. Okamoto, H. Fukushima, K. Okabe, Calcitonin inhibits proton extrusion in resorbing rat osteoclasts via protein kinase A, Pflugers Arch. 445 (2003) 651–658.
[12] A. Gupta, J.C. Edwards, K.A. Hruska, Cellular distribution and regulation of NHE-1 isoform of the NA-H exchanger in the avian osteoclast, Bone 18 (1996) 87–95.
[13] W. Hofstetter, M. Siegrist, A. Simonin, O. Bonny, D.G. Fuster, Sodium/hydrogen exchanger NHA2 in osteoclasts: subcellular localization and role in vitro and in vivo, Bone 47 (2010) 331–340.
[14] N. Nakamura, S. Tanaka, Y. Teko, K. Mitsui, H. Kanazawa, Four Na+/H+ exchanger isoforms are distributed to Golgi and post-Golgi compartments and are involved in organelle pH regulation, J. Biol. Chem. 280 (2005) 1561–1572.
[15] Q. Ouyang, S.B. Lizarraga, M. Schmidt, U. Yang, J. Gong, D. Ellisor, J.A. Kauer, E. M. Morrow, Christianson syndrome protein NHE6 modulates TrkB endosomal signaling required for neuronal circuit development, Neuron. 80 (1) (2013) 97–112.
[16] L. Xinhan, M. Matsushita, M. Numaza, A. Taguchi, K. Mitsui, H. Kanazawa, Na+/H+ exchanger isoform 6 (NHE6/SLC9A6) is involved in clathrin-dependent endocytosis of transferrin, Am. J. Phys. Cell Physiol. 301 (2011) C1431–C1444.
[17] J.K. Hill, C.L. Brett, A. Chyou, L.M. Kallay, M. Sakaguchi, R. Rao, P.G. Gillespie, Vestibular hair bundles control pH with (Na+, K+)/H+ exchangers NHE6 and NHE9, J. Neurosci. 26 (2006) 9944–9955.
[18] K. Kucharava, Y. Brand, G. Albano, M. Sekulic-Jablanovic, A. Glutz, X. Xian, J. Herz, D. Bodmer, D.G. Fuster, V. Petkovic, Sodium-hydrogen exchanger 6 (NHE6) deficiency leads to hearing loss, via reduced endosomal signalling through the BDNF/Trk pathway, Sci. Rep. 10 (2020) 3609.
[19] R. Ohgaki, N. Fukura, M. Matsushita, K. Mitsui, H. Kanazawa, Cell surface levels of organellar Na+/H+ exchanger isoform 6 are regulated by interaction with RACK1, J. Biol. Chem. 283 (2008) 4417–4429.
[20] R. Ohgaki, N. Fukura, M. Matsushita, K. Mitsui, H. Kanazawa, Cell surface levels of organellar Na+/H+ exchanger isoform 6 are regulated by interaction with the receptor for activated C-kinase 1, J. Biol. Chem. 283 (7) (2007) 4417–4429.
[21] A.L. Christianson, R.E. Stevenson, C.H. van der Meyden, J. Pelser, F.W. Theron, P. L. van Rensburg, M. Chandler, C.E. Schwartz, X linked severe mental retardation, craniofacial dysmorphology, epilepsy, ophthalmoplegia, and cerebellar atrophy in a large South African kindred is localised to Xq24-q27, J. Med. Genet. 36 (1999) 759–766.

[22] J.Y. Garbern, M. Neumann, J.Q. Trojanowski, V.M. Lee, G. Feldman, J.W. Norris, M.J. Friez, C.E. Schwartz, R. Stevenson, A.A. Sima, A mutation affecting the sodium/proton exchanger, SLC9A6, causes mental retardation with tau deposition, Brain 133 (2010) 1391–1402.
[23] G.D. Gilfillan, K.K. Selmer, I. Roxrud, R. Smith, M. Kyllerman, K. Eiklid, M. Kroken, M. Mattingsdal, T. Egeland, H. Stenmark, H. Sjoholm, A. Server, L. Samuelsson, A. Christianson, P. Tarpey, A. Whibley, M.R. Stratton, P.A. Futreal, J. Teague, S. Edkins, J. Gecz, G. Turner, F.L. Raymond, C. Schwartz, R.E. Stevenson, D. E. Undlien, P. Stromme, SLC9A6 mutations cause X-linked mental retardation, microcephaly, epilepsy, and ataxia, a phenotype mimicking Angelman syndrome, Am. J. Hum. Genet. 82 (2008) 1003–1010.
[24] Y. Takahashi, K. Hosoki, M. Matsushita, M. Funatsuka, K. Saito, H. Kanazawa, Y. Goto, S. Saitoh, A loss-of-function mutation in the SLC9A6 gene causes X-linked mental retardation resembling Angelman syndrome, Am. J. Med. Genet. B Neuropsychiatr. Genet. 156B (2011) 799–807.
[25] D.G. Winkler, M.K. Sutherland, J.C. Geoghegan, C. Yu, T. Hayes, J.E. Skonier, D. Shpektor, M. Jonas, B.R. Kovacevich, K. Staehling-Hampton, M. Appleby, M. E. Brunkow, J.A. Latham, Osteocyte control of bone formation via sclerostin, a novel BMP antagonist, EMBO J. 22 (2003) 6267–6276.
[26] W. Xie, S. Lorenz, S. Dolder, W. Hofstetter, Extracellular iron is a modulator of the differentiation of osteoclast lineage cells, Calcif. Tissue Int. 98 (2016) 275–283.
[27] N.H. Kelly, J.C. Schimenti, F. Patrick Ross, M.C. van der Meulen, A method for isolating high quality RNA from mouse cortical and cancellous bone, Bone 68 (2014) 1–5.
[28] C. Deisl, A. Simonin, M. Anderegg, G. Albano, G. Kovacs, D. Ackermann, H. Moch, W. Dolci, B. Thorens, A.H. M, D.G. Fuster, Sodium/hydrogen exchanger NHA2 is critical for insulin secretion in beta-cells, Proc. Natl. Acad. Sci. U. S. A. 110 (2013) 10004–10009.
[29] A. Simonin, D. Fuster, Nedd4-1 and beta-arrestin-1 are key regulators of Na+/H+ exchanger 1 ubiquitylation, endocytosis, and function, J. Biol. Chem. 285 (2010) 38293–38303.
[30] D.G. Fuster, R.T. Alexander, Traditional and emerging roles for the SLC9 Na+/H+ exchangers, Pflugers Arch. 466 (2014) 61–76.
[31] C.L. Brett, Y. Wei, M. Donowitz, R. Rao, Human Na(+)/H(+) exchanger isoform 6 is found in recycling endosomes of cells, not in mitochondria, Am. J. Phys. Cell Physiol. 282 (2002) C1031–C1041.
[32] G. Albano, S. Dolder, M. Siegrist, A. Mercier-Zuber, M. Auberson, C. Stoudmann, W. Hofstetter, O. Bonny, D.G. Fuster, Increased bone resorption by osteoclast-specific deletion of the sodium/calcium exchanger isoform 1 (NCX1), Pflugers Arch. 469 (2017) 225–233.
[33] G. Albano, M. Moor, S. Dolder, M. Siegrist, C.A. Wagner, J. Biber, N. Hernando, W. Hofstetter, O. Bonny, D.G. Fuster, Sodium-dependent phosphate transporters in osteoclast differentiation and function, PLoS One 10 (2015), e0125104.
[34] N. Takahashi, T. Akatsu, N. Udagawa, T. Sasaki, A. Yamaguchi, J.M. Moseley, T. J. Martin, T. Suda, Osteoblastic cells are involved in osteoclast formation, Endocrinology 123 (1988) 2600–2602.
[35] B. Masereel, L. Pochet, D. Laeckmann, An overview of inhibitors of Na(+)/H(+) exchanger, Eur. J. Med. Chem. 38 (2003) 547–554.
[36] W. Balemans, M. Ebeling, N. Patel, E. Van Hul, P. Olson, M. Dioszegi, C. Lacza, W. Wuyts, J. Van Den Ende, P. Willems, A.F. Paes-Alves, S. Hill, M. Bueno, F. J. Ramos, P. Tacconi, F.G. Dikkers, C. Stratakis, K. Lindpaintner, B. Vickery, D. Foernzler, W. Van Hul, Increased bone density in sclerosteosis is due to the deficiency of a novel secreted protein (SOST), Hum. Mol. Genet. 10 (2001) 537–543.
[37] M.E. Brunkow, J.C. Gardner, J. Van Ness, B.W. Paeper, B.R. Kovacevich, S. Proll, J. E. Skonier, L. Zhao, P.J. Sabo, Y. Fu, R.S. Alisch, L. Gillett, T. Colbert, P. Tacconi, D. Galas, H. Hamersma, P. Beighton, J. Mulligan, Bone dysplasia sclerosteosis results from loss of the SOST gene product, a novel cystine knot-containing protein, Am. J. Hum. Genet. 68 (2001) 577–589.
[38] K.S. Houschyar, C. Tapking, M.R. Borrelli, D. Popp, D. Duscher, Z.N. Maan, M. P. Chelliah, J. Li, K. Harati, C. Wallner, S. Rein, D. Pforringer, G. Reumuth, G. Grieb, S. Mouraret, M. Dadras, J.M. Wagner, J.Y. Cha, F. Siemers, M. Lehnhardt, B. Behr, Wnt pathway in bone repair and regeneration - what do we know so far, Front. Cell Dev. Biol. 6 (2018) 170.
[39] J.F. Charles, F. Coury, R. Sulyanto, D. Sitara, J. Wu, N. Brady, K. Tsang, K. Sigrist, D.M. Tollefsen, L. He, D. Storm, A.O. Aliprantis, The collection of NFATc1-dependent transcripts in the osteoclast includes numerous genes non-essential to physiologic bone resorption, Bone 51 (2012) 902–912.
[40] F.P. Coxon, A. Taylor, Vesicular trafficking in osteoclasts, Semin. Cell Dev. Biol. 19 (2008) 424–433.
[41] F.M. Perez-Campo, A. Santurtun, C. Garcia-Ibarbia, M.A. Pascual, C. Valero, C. Garces, C. Sanudo, M.T. Zarrabeitia, J.A. Riancho, Osterix and RUNX2 are transcriptional regulators of sclerostin in human bone, Calcif. Tissue Int. 99 (2016) 302–309.
[42] M. Viswanathan, S. Reddy, N. Berkman, K. Cullen, J.C. Middleton, W.K. Nicholson, L.C. Kahwati, Screening to prevent osteoporotic fractures: updated evidence report and systematic review for the US preventive services task force, JAMA 319 (2018) 2532–2551.
[43] D.W. Dempster, J.E. Compston, M.K. Drezner, F.H. Glorieux, J.A. Kanis, H. Malluche, P.J. Meunier, S.M. Ott, R.R. Recker, A.M. Parfitt, Standardized nomenclature, symbols, and units for bone histomorphometry: a 2012 update of the report of the ASBMR Histomorphometry Nomenclature Committee, J. Bone Miner. Res. 28 (2013) 2–17.
[44] K. Kucharava, Y. Brand, G. Albano, M. Sekulic-Jablanovic, A. Glutz, X. Xian, J. Herz, D. Bodmer, D.G. Fuster, V. Petkovic, Sodium-hydrogen exchanger 6 (NHE6) deficiency leads to hearing loss, via reduced endosomal signalling through the BDNF/Trk pathway, Sci. Rep. 10 (1) (2020) 3609, https://doi.org/10.1038/s41598-020-60262-5.
[45] A. Simonin, D. Fuster, Nedd4-1 and beta-arrestin-1 are key regulators of Na+/H+ exchanger 1 ubiquitylation, endocytosis, and function, J. Biol. Chem. 285 (49) (2010) 38293–38303, https://doi.org/10.1074/jbc.M110.115089.
[46] M. Bargagli, N.A. Dhayat, M. Anderegg, M. Semmo, U. Huynh-Do, B. Vogt, P. M. Ferraro, D.G. Fuster, Urinary Lithogenic Risk Profile in ADPKD Patients Treated with Tolvaptan, Clin. J. Am. Soc. Nephrol. 15 (7) (2020) 1007–1014, https://doi.org/10.2215/CJN.13861119.